A Comparative Analysis on the Static Properties of 'Five-tier Outer Eave Column-head Dougong Bracket' from the Main Hall of Chuzu Convent in Song Dynasty

Yuanhe Li,[a] Hongfa Kang,[a] and Lihong Yao [b,*]

This research explored the static structural behavior of the Song Dynasty 'Five-tier Outer Eave Column-head Dougong Bracket' in the Main Hall of Chuzu Convent. Finite element analysis (FEA) was employed. Relying on an orthotropic constitutive model and *Pinus sylvestris'* mechanical properties, a refined ANSYS model was built (assessed in line with GB/T criteria), with the Hill yield criterion to evaluate wood plasticity. For assessing strength, deformation and energy dissipation, simulations were carried out involving Z-axis vertical monotonic static loading and X/Y-axis horizontal low-count reciprocating loading. The findings showed a vertical ultimate bearing capacity of 342 kN along the Z-axis. Stress concentrations peak at 18.8 MPa specifically at the capital block-Ludou junction, a significant concern. Horizontal loading resulted in symmetrical hysteresis loops, exhibiting peak thrusts: 750 kN (Y-axis) and 597 kN (X-axis). Ductility coefficients (4.98/Y, 3.67/X) and equivalent viscous damping coefficients (0.121/Y, 0.149/X) were identified. The vertical behavior followed a tri-linear stiffness degradation model, with the horizontal response adhering to multi-linear restoring force models. The findings confirm FEA as an efficient, reliable method to assess Dougong mechanical behavior, providing crucial knowledge for ancient wooden building upkeep.

DOI: 10.15376/biores.21.2.4357-4374

Keywords: Dougong bracket; Chuzu Convent; Static characteristics; Finite element simulation; Pinus sylvestris

*Contact information: a: School of Architecture and Art Design, Inner Mongolia University of Science & Technology, Baotou 014010, P.R. China; b: School of Material Science and Art Design, Inner Mongolia Agricultural University, Hohhot 010018, P.R. China; *Corresponding author: yaolihong@imau.edu.cn*

INTRODUCTION

The main hall of Chuzu Temple (Fig. 1), located in Dengfeng District, Henan province, China, is one of the famous national key cultural relic's protection units. Constructed in 1125 CE during the Song Dynasty, it is one of the earliest surviving ancient Chinese wooden structures in Henan Province. The Chinese Society of Architecture has conducted in-depth research on the main hall of the Chuzu Temple and believes that it is an important example reflecting the architectural technology of the Song Dynasty. Its architectural approach is very close to the regulations of the 'Rules of Architecture Noted', providing valuable physical materials for our study of Song Dynasty architecture. It has significant historical value and academic significance (Yao *et al.* 2019).

Fig. 1. The main hall of the Chuzu Convent

Dougong is the core load-bearing and anti-seismic component of traditional wood structures in East Asia (especially Chinese traditional wood structures), and its design and mechanical performance are the key points for traditional buildings to withstand the millennium earthquake test. It is not a single functional component; rather it is an integrated unit of 'load-bearing force transmission seismic resistance' in traditional wooden structures, with the ability of 'deformation coordination' and 'self-resetting' (Suzuki and Maeno 2006; Bedon *et al.* 2015; Yeo *et al.* 2016; Wang *et al.* 2022). 'Paving' is the official name of the Song Dynasty for *Dougong*, which refers to the load-bearing and decorative components composed of 'Dou' (square spacer), 'Gong' (strip crossbar), 'Ang' (oblique member), *etc*. The core function is to 'transmit the roof load to the columns/foreheads', while adjusting the proportions of the building and reflecting the grade. In the Song Dynasty, the 'number of paving' is equal to the number of jumps plus 3 ('jumping' refers to the number of horizontal/oblique component layers protruding outward/inward from the bucket arch), which is the core index for judging the complexity of the bucket arch. The eight-tier (out of 5 jumps) is the highest-level bucket arch shape in the existing ancient Chinese wooden buildings. The five-tier (out of 2 jumps) studied in this paper effectively avoids the functional limitations caused by the small number of jumps and can prevent the component redundancy caused by the large number of jumps (Fig. 2).

Fig. 2. The authentic Five-tier outer eave column-head dougong bracket in the Chuzu Convent Gate

Nomenclature follows a codified relationship. Five paving refers to starting from the lowest layer of *Ludou* (the bottom bucket of the bucket arch), with 5 layers of core components (dou plus gong/ang) and 2 layers of components protruding outward. Heavy arch refers to the superimposition of two layers of *Gong* on the same 'jump' of the bucket arch. 'Single chao' is one layer of horizontal arches extending outward, and 'single ang' is above the 'single chao', and then extends outward by one layer diagonally. The outer side is used as the counting benchmark to form the pillar head Dougong of the Chuzu temple hall, reflecting the grandeur of the Song Dynasty bucket arch.

Following the modular system prescribed in Yingzao Fashi (Treatise on Architectural Methods, Song Dynasty), Dougong brackets are classified into eight grades based on dimensional hierarchies, each with distinct scale factors tailored to buildings of varying magnitudes (Van and John 2008; Wu *et al.* 2020; Sha *et al.* 2021). In accordance with Yingzao Fashi (Song Dynasty architectural treatise), the dougong bracket examined in this study corresponds to the third-grade timber within the cai-fen modular system (Chen *et al.* 2025). As stipulated in the treatise, one fen° unit for the third-grade timber is defined as 15.5 mm. Specifically, the research examines the outer eaves and capital Dougong bracket of the main hall of the Chuzu Convent, comprising 53 modular units—33 primary members and 20 wooden pins—categorized into three types. Figures 3 and 4 show the test model's perspective view and exploded assembly diagram, delineating its hierarchical composition.

Fig. 3. The perspective view of the Chuzu Convent's test model for the 'Five-tier Outer Eave and Capital Block Dougong Bracket'

The experimental investigation of traditional timber structures faces significant economic challenges, particularly in constructing full-scale Dougong bracket models, which require substantial material and labor investments (Meng *et al.* 2019; Zhang *et al.* 2024). Traditional mechanical tests are mostly based on limited measuring points. The test results are easily affected by system errors, and the spatial resolution is insufficient. These problems will further weaken the reliability and accuracy of data in complex structural systems. Finite element analysis (FEA) has emerged as a robust computational tool for characterizing Dougong mechanics, reduce the influence of system error and spatial resolution limitation, and improve the accuracy and reliability of mechanical characterization results (Meng *et al.* 2018; Sha *et al.* 2021; Wu *et al*. 2022; Xue *et al.* 2022; Sejkot *et al.* 2024). This paradigm shift offers dual advantages: (1) elimination of physical specimen fabrication costs, and (2) precise control over boundary conditions and material anisotropy, enabling targeted analysis of critical structural interfaces (Song *et al.* 2019; Zhang *et al.* 2023).

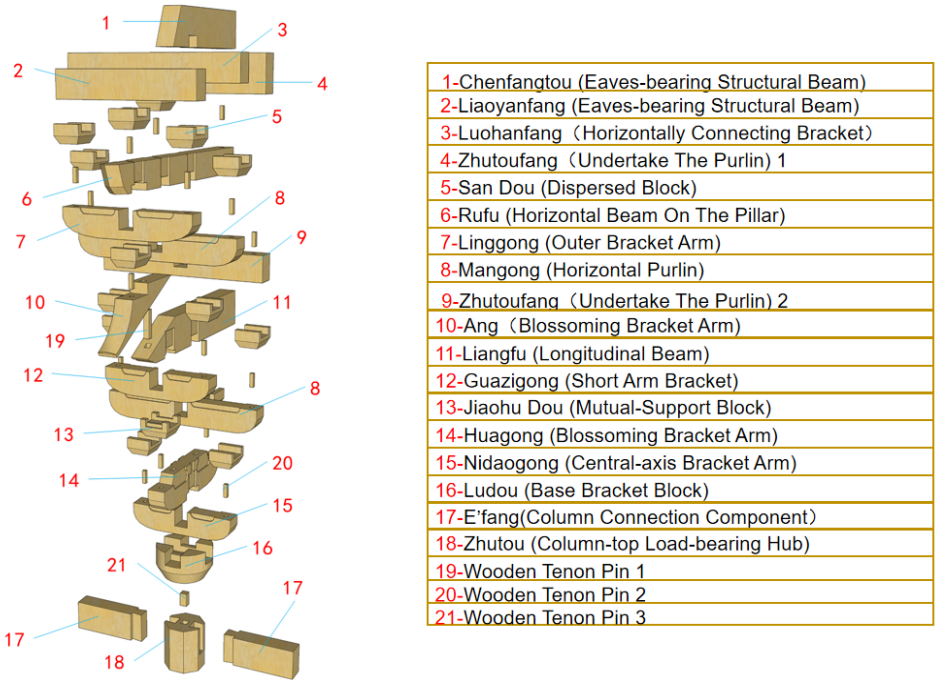

Fig. 4. The exploded assembly diagram of the 'Five-tier Outer Eave and Capital Block Dougong Bracket' test model at Chuzu Convent

This study employs a high-fidelity finite element analysis (FEA) framework to explore the static behavior of a Five-tier Outer Eave and Capital block Dougong bracket. Taking the bucket arch of the five-story outer eaves of the Song Dynasty as the research object, the static structural behavior is revealed, and the rationality and reliability of the finite element simulation method applied to the stress analysis of the Dougong are verified. The computational model integrates three essential mechanical parameters: (1) strength properties (maximum load capacity and stress distribution patterns); (2) mechanisms of deformation (decrease in stiffness and displacement gradients); and (3) energy dissipation (hysteretic energy absorption and equivalent viscous damping). Thorough simulations of vertical (Z-axis) monotonic and horizontal (X/Y-axis) low-cycle loading protocols, The approach showcases a strong alignment with empirical data from physical tests, while simultaneously achieving substantial cost savings in experimentation. It makes up for the lack of attention to the static mechanical behavior of specific heritage timber structures such as the five-tier outer eave capital block bracket.

EXPERIMENTAL

Finite Element Simulation

The finite element model employed *P. sylvestris* timber that had been conditioned to a moisture content of 12%. The mechanical characteristics were established by conducting standardized examinations. The air-dry density was 0.493 g/cm³ (GB/T 1933 2009), and the elastic moduli (E) and Poisson's ratios (v) were determined. The shear moduli (G) were quantified using strain gauge methods as per GB/T 15777 (2017), GB/T 1943 (2009), and LY/T 3297 (2022). The strength tests demonstrated a longitudinal

compressive strength of 35.2 MPa (GB/T 1935 2009) and a transverse compressive strength of 5.14 MPa (GB/T 1939-2009). The flexural strength of the material was 52.9 MPa (GB/T 1936.1 2009), as detailed in Table 1.

A finite element model of the Dougong bracket was developed in ANSYS Workbench 2021 R1 employing a multi-physics framework. The calibration of material parameters was conducted based on experimental data, and the modeling of plasticity was done using Hill's anisotropic yield criterion while elasticity was modeled through orthotropic constitutive relations (Yao and Li 2023). The nine elastic constants define the orthotropic behavior of timber: Three Young's modulus values (E_L, E_R, E_T), trashier modulus values (V_{LR}, V_{LT}, V_{RT}), and three Poisson's ratios (G_{LR}, G_{LT}, G_{RT}) are considered. In order to improve the computational efficiency and model stability, the model is simplified reasonably: the wood is defined as an orthotropic defect-free continuum, the interface friction is ignored, the mortise and tenon joints are assumed to be completely combined, and the geometric and material symmetry conditions are adopted.

Table 1. Elastic Modulus, Poisson's Ratio, and Shear Modulus of *P. sylvestris*

	E_L	E_R	E_T	V_{LR}	V_{LT}	V_{RT}	G_{LR}	G_{LT}	G_{RT}
P. sylvestris	8023	1103	843	0.422	0.513	0.687	652	345	231

* E_L denotes the linear elastic modulus, which is measured in megapascals (MPa). The term E_R represents the horizontal radial elastic modulus, which is measured in units of MPa. The horizontal tangential elastic modulus, denoted by E_T, has a unit of MPa. The V_{LR} represents the Poisson's ratio associated with longitudinal extension stress. The Poisson's ratio connected to transverse radial extension stress is denoted as V_{LT}, while the Poisson's ratio related to transverse tangential extension stress is represented by V_{RT}. G_{LR} denotes the longitudinal-radial shear modulus, which is measured in MPa. The G_{LT} represents the longitudinal-chordal shear modulus, which is measured in megapascals (MPa). G_{RT} represents the horizontal shear modulus, which is measured in MPa.

Loading Protocol

The experimental loading protocol followed the coordinate system established in Fig. 5. In the vertical loading scenario, forces (Cao *et al.* 2023) were applied along the Z-axis to mimic permanent roof loads in a monotonic static manner. Bidirectional low-count reciprocating displacements (Lin *et al.* 2022; Wang *et al.* 2022). The instructions for the year 2022 were given in parallel with the Y- and X-axes to mimic seismic movements.

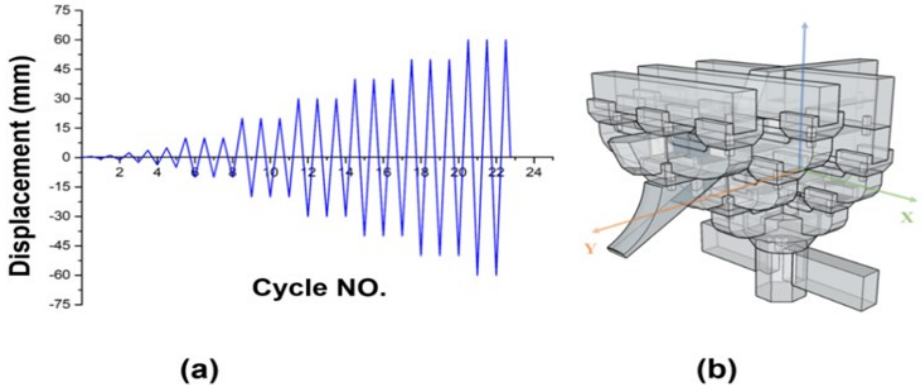

Fig. 5. The loading protocol (a) and orientation specification of the test model in the coordinate axes (b)

Following the experimental methodology proposed by Niu (2017), the researchers conducted perpendicular monotonic static loading tests to simulate the transfer mechanism of permanent roof loads in Chinese heritage Dougong systems. A vertical load of 60 kN was initially applied, which corresponds to the calculation based on the perpetual roof load specified in the load specification and determined through structural analysis. The experiment was carried out employing a hybrid-displacement control approach and executed in two consecutive stages. In the initial phase, a steady force of 5 kN/min was applied to regulate the load until the specimen attains a yield state, which is determined by observable deformation or significant nonlinear characteristics in the load-displacement response. Following the initial phase, the test moved on to the second stage, which was conducted under displacement control at a rate of 2 mm/min in order to assess post-yield performance. The termination criteria during this phase encompassed either structural collapse, which was defined as a decrease in load capacity down to 80% of the peak resistance, or significant damage that hindered further loading. This two-phase methodology allowed for comprehensive documentation of both elastic and plastic deformation characteristics. Simultaneously, it can guarantee a monitored examination throughout the entire failure process. Accurate data support is provided for the analysis of deformation laws and failure mechanisms.

A displacement control method was employed to conduct quasi-static tests, which were carried out under horizontal low periodic reciprocating loads (Yao and Li 2023). The starting phase consists of five monotonic reciprocating cycles with amplitudes that gradually increase (0.0125Δ, 0.025Δ, 0.05Δ, 0.075Δ, and 0.1Δ, where Δ is equal to 50 mm). The secondary phase comprises three reciprocal cycles at each amplitude level, beginning from 0.2Δ. At each step, the amplitude is increased incrementally by 0.2Δ (Bedon *et al.* 2015). The loading protocol is depicted in Fig. 5A. The solver setup, interconnections of components, and boundary conditions are meticulously aligned with the experimental parameters along the Z-, Y-, and X-axes (Fig. 5b).

Grid System

The grid system was built using second-order elements and employed a hybrid meshing strategy that combined hexahedral and tetrahedral shapes. Geometrically, regular regions were divided into hexahedral elements, while complex geometric regions utilize tetrahedral elements. The grid system that emerged following the completion of the Dougong bracket's final assembly is depicted in Fig. 6.

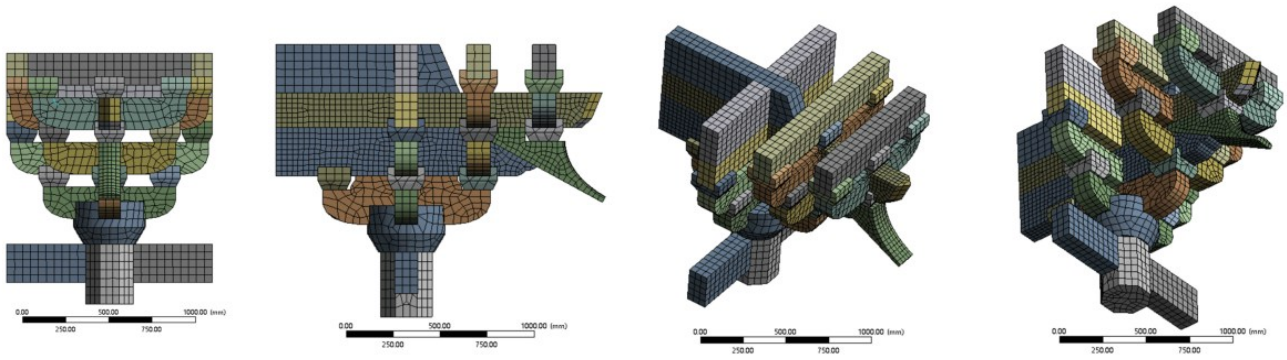

Fig. 6. Division of Dougong bracket's grid systematic in simulation

RESULTS AND DISCUSSION

Vertically-oriented Monotonic Static Loading (along the Z-axis)

The load-displacement curve obtained from the perpendicular monotonic loading simulation along the Z-axis is shown in Fig. 7. The simulation of the Dou-Gong bracket model shows that its bearing capacity fails to converge once it reaches 342 kN. Under the Z-axis loading, the equivalent stress of the vertical monotonic loading of the bucket arch in Song Dynasty.

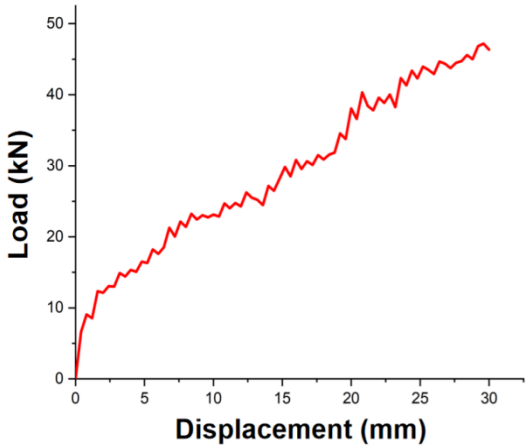

Fig. 7. The load-displacement curve along the Z-axis

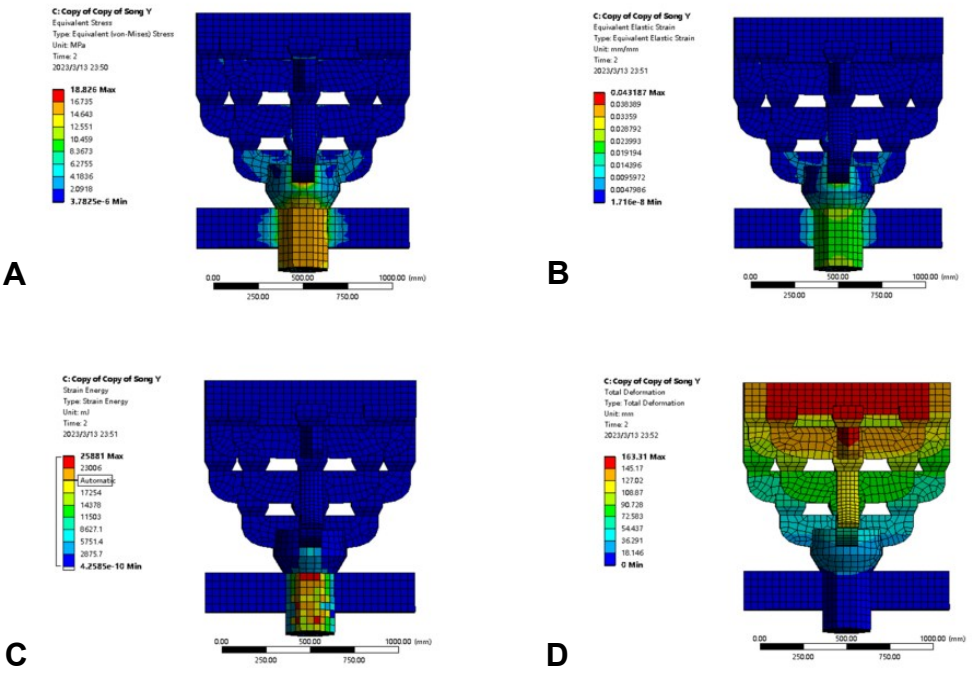

Fig. 8. The distribution of Von Mises stress, equivalent elastic strain distribution, strain energy density distribution, and displacement analysis along the Z-axis

The distribution of Fig. 8A is primarily found in the Ludou and column head areas. The maximum stress level of 18.826 MPa was predominantly observed at the junction between the column head and the Ludou. This refers to the core mortise-tenon joint. In the equivalent elastic strain distribution (Fig. 8B), similar distribution patterns were found, where the peak strain reached up to 0.043 at this crucial structural junction. The strain energy density distribution (Fig. 8C) showed spatial correlation with stress concentrations, and a significant amount of 25881 MJ was observed to accumulate at the Ludou-column head joint. The concentration of energy observed in this phenomenon serves as evidence that the arch in wooden architecture efficiently channels upper energy to the column. Displacement analysis (Fig. 8D) showcased a gradual reduction in deformation gradient, starting from 163.31 mm at the top of Liaoyanfang. When traditional timber structures are subjected to vertical loads, their anisotropic characteristics come into play.

Horizontally-Oriented Low-Cycle Reciprocating Loading (along the Y-axis and X-axis)

The load-displacement hysteretic behavior of the Dougong bracket is illustrated in Fig. 9, which presents the simulation results of the horizontal low-cycle reciprocating load tests along the Y and X axes. The experimental model demonstrates a peak lateral load capacity of 750 kN (Y-axis) and 597 kN (X-axis). With symmetrical full spindle-shaped patterns shown in both axial hysteresis curves, the model exhibits significant plastic deformation capacity and remarkable energy dissipation efficiency under cyclic loading.

The load-displacement skeleton curve can be obtained from the hysteretic curve (Fig. 10), while the specimen's stiffness degradation curve is created by extracting stiffness values from each segment of the skeleton curve (Fig. 11).

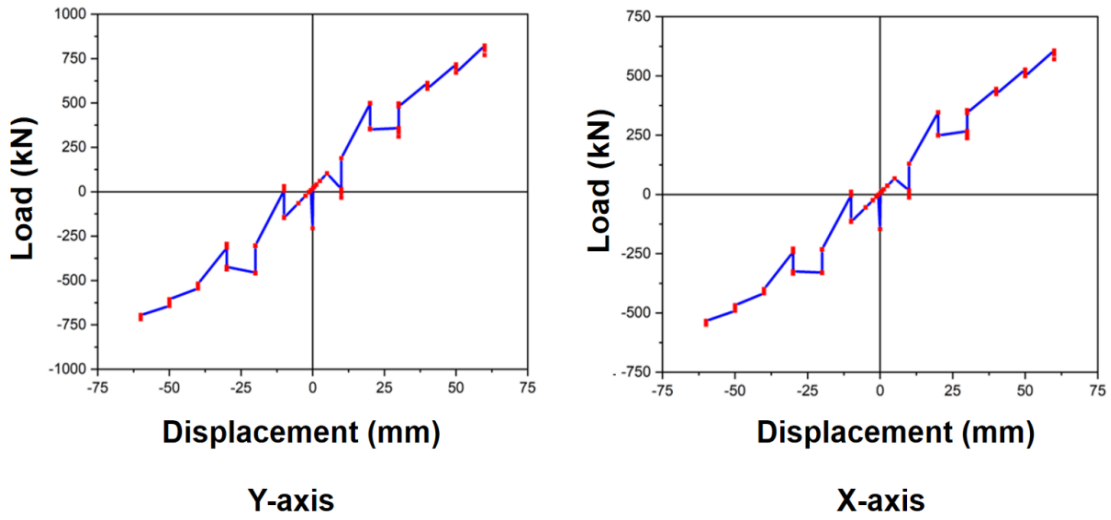

Fig. 9. The load-displacement hysteretic curves along the Y-axis and X-axis

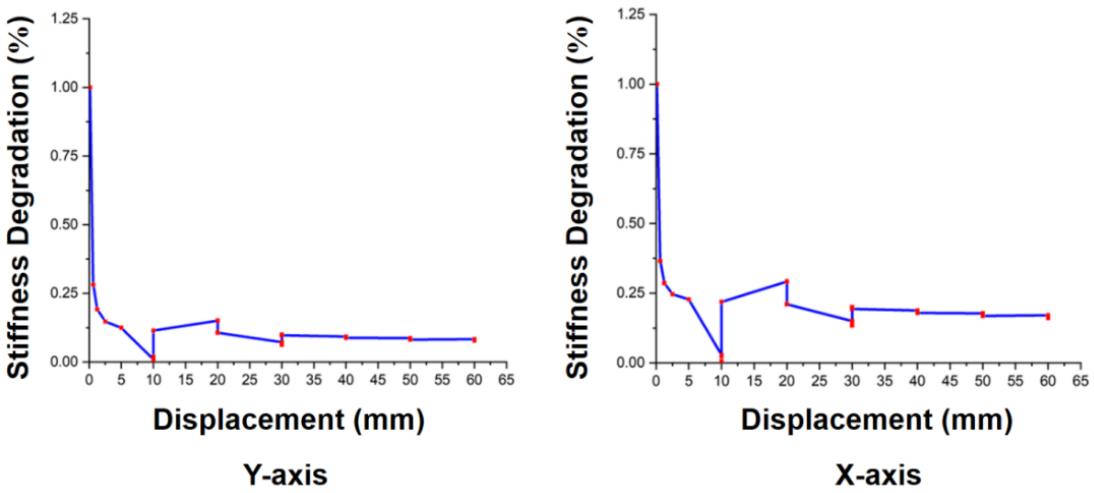

Fig. 10. The load-displacement skeleton curves along the Y-axis and X-axis

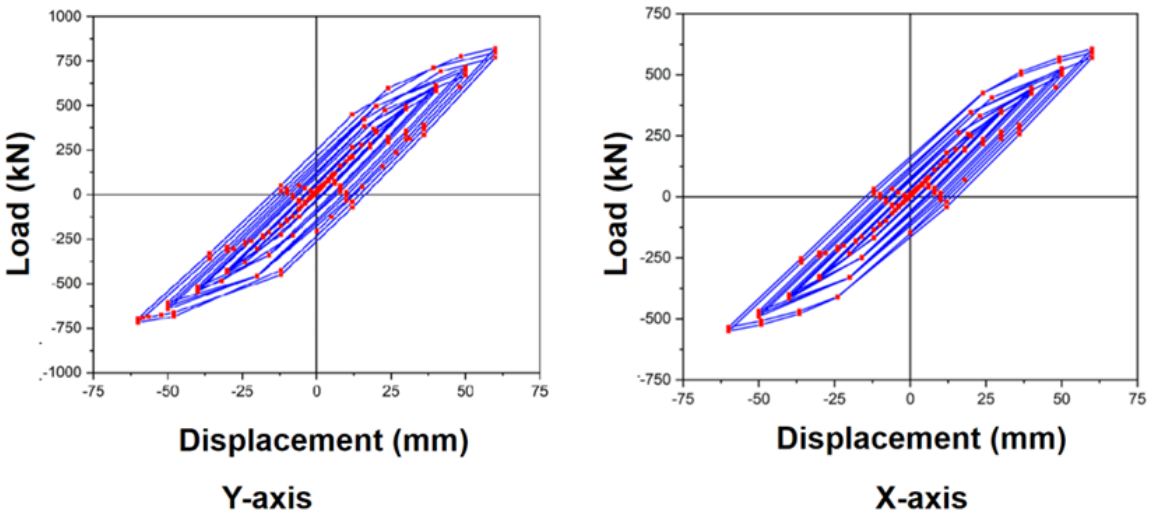

Fig. 11. The stiffness degradation curves along the Y-axis and X-axis

The Von Mises stress distribution (Fig. 12A) reveals pronounced stress accumulation, which is primarily concentrated at the rear region of the component, particularly in the rear section of the Huagong and the column head. The maximum stress intensity reaches 50.7 MPa, and it is specifically located at the mortise-tenon joint between the rear end of the beam and the Sandou. A consistent spatial distribution pattern is also observed in the equivalent elastic strain (Fig. 12B). The maximum equivalent elastic strain is 0.0590, which is also concentrated at the mortise-tenon joint between the rear end of the beam and the Sandou.

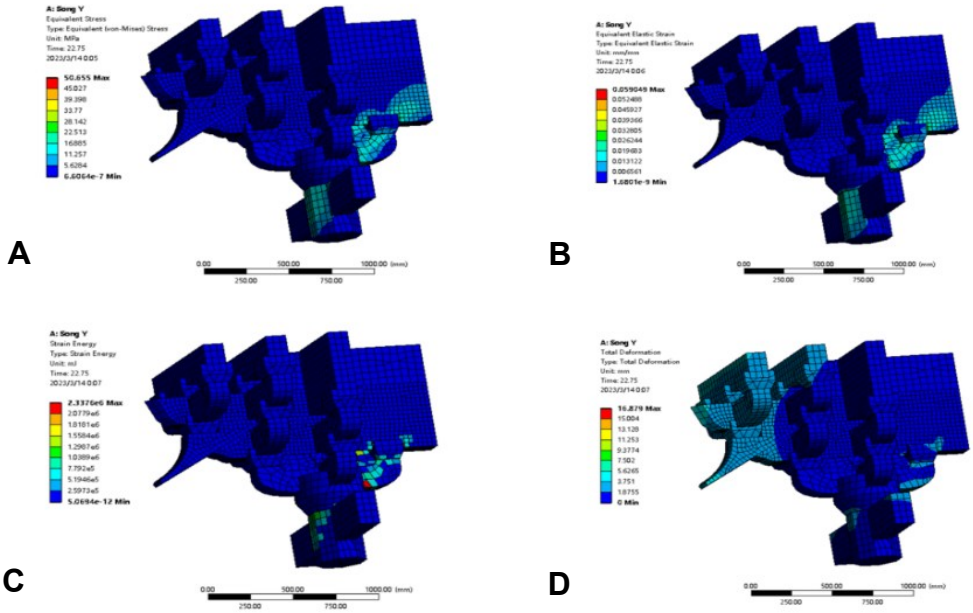

Fig. 12. Distribution of von Mises stress, equivalent elastic strain, strain energy density, and Y-axis-oriented displacement analysis

Strain energy density distribution (Fig. 12C) demonstrated topological congruence with the stress field, confirming efficient energy transmission through the arch-rafters-bucket structural system to the supporting columns. The highest amount of accumulated strain energy, reaching 2.34×10^6 MJ, was observed at the tenon-mortise joint located between the back end of the beam and the *Sandou*. This area is recognized as the primary site for energy dissipation. Analysis of displacement (Fig. 12D) exhibited a deformation pattern characterized by a hierarchical organization. The maximum displacement reached 16.9 mm at the tenon-mortise joint located between the rear end of the beam and the *Sandou*, with the secondary deformation gradient being spread out evenly across all regions in the Linggong. The connection point between the *Huagong* rear section and the beam, as well as the interface between *Ludou* and the column head, are both crucial junctions.

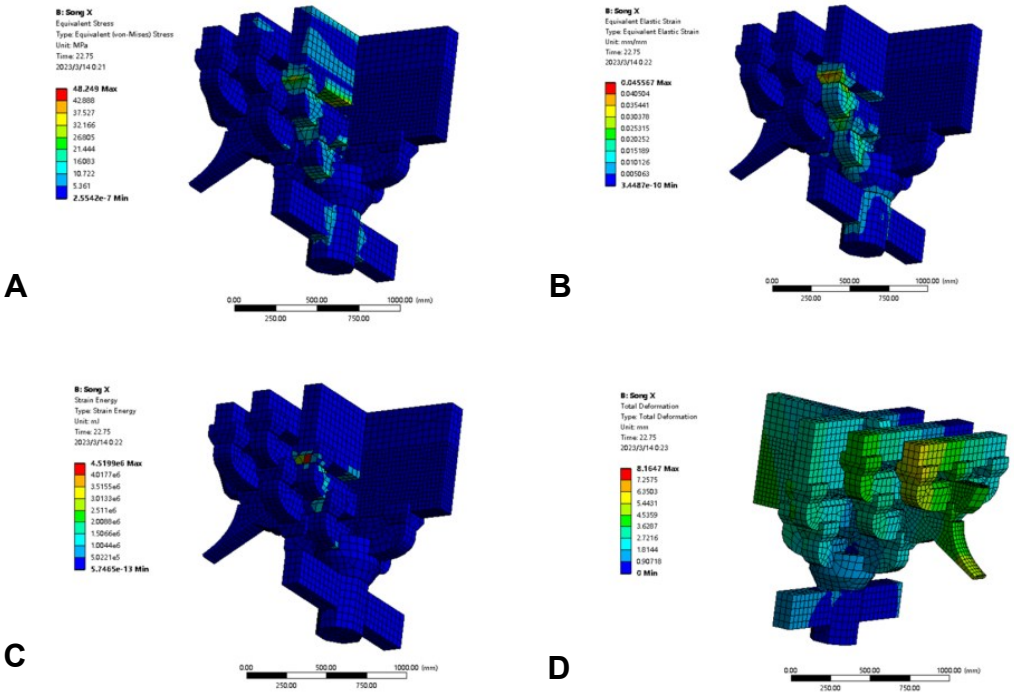

Fig. 13. Analysis of Von Mises stress distribution, equivalent elastic strain distribution, strain energy density distribution, and X-axis-aligned displacement

The distribution of Von Mises stress (Fig. 13A) under quasi-static loading in the X-axis direction revealed critical stress concentration at the mortise-tenon joint located at the connection point of the *Mangong* and the *Sandou*, with peak stress value amounting to 48.2 MPa. This stress localization is correlated with the distribution of equivalent elastic strain (Fig. 13B), which showed maximum magnitudes of 0.0455 at the mortise-tenon joint located at the connection point of the *Mangong* and the *Sandou*, verifying the spatial consistency between the stress field and the strain field. The strain energy density distribution, meanwhile (Fig. 13C) reflected the stress concentration distribution pattern, accumulating 4.52×10^6 MJ at the mortise-tenon joint located at the connection point of the *Mangong* and the *Sandou*. This energy concentration indicates that the mortise-tenon joint functions as the primary energy dissipation zone under cyclic loading. Displacement analysis (Fig. 13D) revealed maximum deformation of 8.16 mm at the mortise-tenon joint located at the connection point of the *Mangong* and the *Sandou*, while the structural deformation gradients diminished gradually toward the foundation, which aligns with the deformation mechanisms of traditional timber structures under lateral loading. Of note, the integrated stress-strain-energy triad signals the potential initiation of failure at the mortise-tenon joint located at the connection point of the *Mangong* and the *Sandou*, where both mechanical stress and strain energy density surpass the critical thresholds seen in similar timber joints. This failure mechanism corresponds to the documented damage modes in historical timber structures subjected to cyclic lateral loads

A Comprehensive Mechanical Model for Analyzing the Static Structural Response in Three Dimensions (X-axis, Y-axis, Z-axis)

The five-tier outer eave and capital block Dougong bracket displayed a tri-linear elastic stiffness degradation behavior pattern when subjected to Z-axis monotonic loading (Fig. 14). The material under investigation demonstrates three distinct mechanical phases. During the initial stage of Phase OA (0–ΔA), the process of closing the gaps between various components leads to the emergence of contact nonlinearity. This results in a relatively low structural stiffness, as indicated by the KOA value of 4.42 kN/mm, which was calculated using Eq. 1. During phase AB (ΔA–ΔB), the material exhibits linear elastic behavior with a stabilized stiffness of K_{AB} = 2.37 kN/mm, as calculated using Eq. 2, characterized by fully developed interactions between components. Progressive stiffness degradation (K_{BC} = 1.98 kN/mm, in accordance with Eq. 3. The main characteristic of Phase BC (ΔB–ΔC) arises from the yielding of mortise-tenon joints and the accumulation of structural damage.

$$k_{OA} = \frac{P_x}{\Delta_x} \quad (1)$$

$$k_{AB} = \frac{P_y - P_x}{\Delta_y - \Delta_x} \quad (2)$$

$$k_{BC} = \frac{P_b - P_y}{\Delta_b - \Delta_y} \quad (3)$$

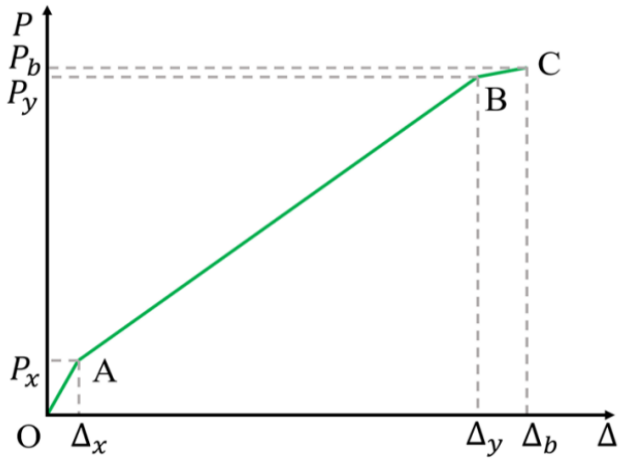

Fig. 14. The tri-linear model of elastic stiffness degradation under Z-axis monotonic loading

Based on the hysteresis curve and skeleton curve, the restoring force model Fig. 15). A test model for the static structural behavior of the five-tier outer eave and capital block Dougong bracket has been developed along both the X-axis and Y-axis. Along the Y-axis, OA represents the elastic stage, in which the displacement of the test model is roughly proportional to the applied load, exhibiting a stiffness of K_{Y1} = 28.11 kN/mm. The AB stage denotes the yield phase, extending from Point A to Point B. During this stage, the model demonstrates plastic behavior, with its stiffness (K_{Y2}) measuring 7.47 kN/mm. The effective stiffness of the Dougong bracket is defined as K_{Y3}, which represents the ratio between the restoring force model's maximum bearing capacity and its maximum displacement. The effective stiffness K_{Y3} for the test model measures 14.84 kN/mm.

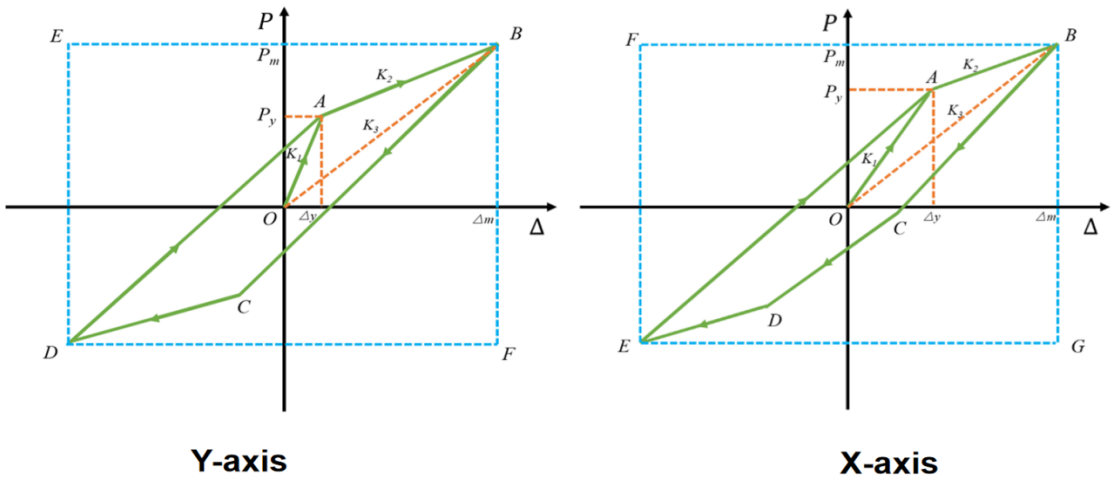

Fig. 15. The restoring force model of static structural behavior along the X-axis and Y-axis

Considering the Dougong bracket component as a means of energy dissipation between the roof and columns in traditional Chinese timber buildings, to quantitatively evaluate its damping performance, the nonlinear coefficient (NL) can be incorporated. The value of NL is determined by calculating the ratio between the envelope area of the restoring force model and the rectangular area S_{BDEF} depicted in Fig. 16. The Dougong bracket's energy dissipation capacity is characterized by NL. The nonlinear coefficient NL of the five-tier outer eave and capital block Dougong bracket test model in the Y-axis direction is 0.201. The coefficient NL in the X-axis direction exhibits nonlinearity with a value of 0.238.

The measure of a Dougong bracket's maximum displacement relative to its yielding displacement is referred to as the component's ductility. A higher level of ductility signifies that the component has an enhanced ability to undergo deformation. The flexibility of the five-tier outer eave and capital block Dougong bracket test model in the Y-axis direction is 4.98. According to the simulation findings, the ductility along the X-axis direction amounts to 3.67.

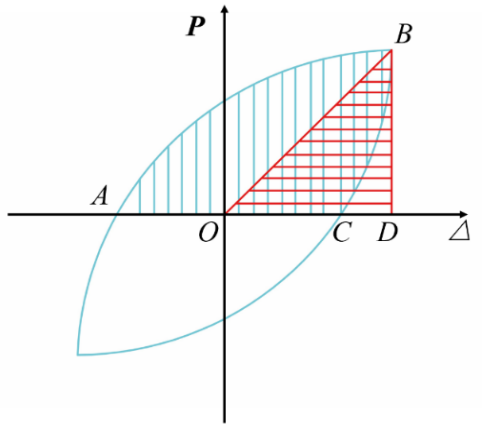

Fig. 16. Determination of the equivalent viscous damping coefficient

$$h_e = \frac{1}{2\pi} \cdot \frac{S_{ABC}}{S_{OBD}} \quad (4)$$

The viscous damping coefficient (h_e) is directly related to the energy dissipation capability of the Dougong bracket component, with a positive correlation. The bigger the value of h_e, the more substantial the capacity. The value of the coefficient is obtained through the analysis presented in Fig. 16 and Eq. 4. In the case of the five-tier outer eave and capital block Dougong bracket test model, the values for the he is 0.121 in the Y-axis direction and 0.149 in the X-axis direction, respectively.

Through three-dimensional analysis (covering the X-, Y-, and Z-axes), the static structural performance and stress-deformation characteristics of the five-tier outer eave capital block Dougong bracket test model (from the Main Hall of Chuzu Convent, Song Dynasty) were evaluated. Under vertical monotonic static loading along the Z-axis, the structural response accords with a variable-stiffness linear elastic model, characterized by three distinct mechanical phases: Phase I involves the initial compaction of inter-component gaps and nodal connections, which prepares the structure for subsequent load-bearing; Phase II demonstrates a linear load-displacement relationship with stable stiffness, embodying the model's elastic load-bearing capacity within this stage; and Phase III culminates in structural yielding that eventually results in ultimate failure, signifying the structure's transition from elastic to plastic deformation.

Table 2. Characteristic Values of the Six Specimen Configurations

Name	Five-tier Outer Eave Capital Block Dougong Bracket from the main hall of the Chuzu Convent in the Song Dynasty					
Pathway	Numerical simulation					
Intensity		Deformation			Energy dissipation	
F_{Z1}	F_{Z2}	K_{Z1}	K_{Z2}	K_{Z3}	NL(Y)	
305.73	342.36	4.42	2.37	1.98	0.201	
F_{Y1}	F_{Y2}	K_{Y1}	K_{Y2}	K_{Y3}	NL(X)	
749.88	749.88	28.11	7.47	14.84	0.238	
F_{X1}	F_{X2}	K_{X1}	K_{X2}	K_{X3}	H_Y	
597.31	597.31	32.37	5.74	12.56	0.121	
		U_Y	U_X		H_X	
		4.98	3.67		0.149	

*The term F_{Z1} refers to the yield bearing capacity in relation to Z-axis loading (measured in kN), whereas F_{Z2} signifies the ultimate bearing capacity concerning Z-axis loading (also measured in kN).In the context of Y-axis loading, F_{Y1} signifies the highest positive horizontal thrust while F_{Y2} denotes the maximum negative horizontal thrust (unit: kN).*In the context of X-axis loading, F_{X1} and F_{X2} denote the maximum positive/negative horizontal thrust, with F_{X1} representing the positive value and F_{X2} representing the negative value, respectively (unit: kN).*
Regarding stiffness parameters: K_{Z1} represents the initial rigidity of the component subjected to Z-axis loading (unit: The yield stiffness under Z-axis loading is represented by K_{Z2} (unit: kN/mm), while the ultimate stiffness under Z-axis loading is denoted by K_{Z3} (unit: kN/mm).In terms of Y-axis loading, K_{Y1} represents the elastic stiffness (unit: kN/mm), K_{Y2} denotes the plastic stiffness (unit: kN/mm), and K_{Y3} signifies the effective stiffness (unit: kN/mm).In the context of X-axis loading, K_{X1} denotes the elastic stiffness (measured in kN/mm), K_{X2} signifies the plastic stiffness (also measured in kN/mm), and K_{X3} stands for the effective stiffness (with units of kN/mm).
Furthermore, U_Y signifies the component's ductility in the Y-axis direction, while U_X denotes its ductility along the X-axis.NL(Y) and NL(X) represent the nonlinear constants associated with the component in the Y-axis and X-axis directions, respectively; The equivalent viscous damping coefficients of the component in the Y-axis and X-axis directions are denoted by H_Y and H_X, respectively.

Under horizontal low-cycle reversed loading along the X- and Y-axes, the structural behavior conforms to a multi-linear restoring force model, progressing sequentially through the elastic, yielding, and failure stages. Moreover, the loading process reveals progressive stiffness degradation exhibited by the Dougong bracket system. Hysteresis loops exhibit pinching characteristics in the vicinity of the origin, which is indicative of interfacial slippage between components. Furthermore, post-critical horizontal loading triggers extensive plastic deformation, coupled with rapid displacement amplification. Key mechanical parameters—assessed triaxially across the dimensions of strength, deformation capacity, and energy dissipation efficiency—are systematically summarized in Table 2. Experimental findings indicate that under excessive loading, structural damage originates at critical structural nodes, and the subsequent redistribution of internal forces triggers progressive collapse of the structural system.

CONCLUSIONS

1. The static structural behavior of the 'Five-tier Outer Eave Capital Block Dougong Bracket' test model from the Chuzu Convent (Song Dynasty) under vertical monotonic static load along the Z-axis can be characterized by a variable stiffness linear elastic mechanical model. Under quasi-static low-cycle reversed loading along the X- and Y-axes, the restoring force model can be used to characterize the static structural behavior of the Dougong bracket component.
2. From the viewpoint of strength, the crucial mechanical characteristics of the Song Dynasty Dougong Bracket test model are as follows: The maximum load capacity and ultimate load capacity along the Z-axis are 306 kN and 342 kN, respectively. The peak horizontal force exerted in the Y-axis direction is 750 kilonewtons. The maximum forward horizontal thrust along the X-axis direction amounts to 597 kN.
3. At the level of deformation, the crucial stiffness and ductility parameters for the Song Dynasty Dougong Bracket test model, based on axis, are as follows: Regarding the Z-axis, the initial stiffness measures at 4.42 kN/mm, while the yield stiffness is recorded as 2.37 kN/mm, and the deformation stiffness is observed to be 1.98 kN/mm. In the vertical direction (Y-axis), it demonstrates a stiffness of 28.1 kN/mm in an elastic manner. The plastic stiffness measures at 7.47 kN/mm, the effective stiffness is recorded as 14.5 kN/mm, and a ductility value of 4.98 is noted. In the X-axis direction, the elastic stiffness measures 32.4 kN/mm, while the plastic stiffness is recorded at 5.74 kN/mm. Consequently, the effective stiffness in this direction amounts to 12.6 kN/mm. The value of ductility is 3.67.
4. At the energy level, the crucial energy parameters of the Song Dynasty Dougong Bracket test model are outlined below: The Y-axis nonlinear coefficient and equivalent viscous damping coefficient are respectively 0.201 and 0.121. The X-axis nonlinear coefficient is 0.238, while the equivalent viscous damping coefficient is 0.149.

5. The finite element method (FEM) effectively validated the structural efficacy of the Dougong bracket via comprehensive mechanical indicators. Specifically, the maximum load that can be supported is 342 kN, while the flexibility along the Y-axis measures 4.98 and along the X-axis it is 3.67. The Song Dynasty craftsmen's design was confirmed to be a mechanically optimized solution that achieved a balance between load transfer efficiency and seismic resilience. This study demonstrates that modern numerical simulation can be responsibly applied to reveal the inherent structural wisdom of historical buildings, thereby supporting the scientific and sustainable protection of precious cultural relics.

ACKNOWLEDGMENTS

This work was supported by the National Natural Science Foundation of China-Regional Science Foundation Project 'Construction of Static Structural Performance Evaluation System for Five-tier Outer Eave Column-head Dougong Bracket Components (32360356), the Scientific Research Projects of First-class Disciplines (Grant No. YLXKZX-NKD-027), and the Fundamental Research Funds for Inner Mongolia University of Science & Technology (Grant No. 2024QNJS023).

REFERENCES CITED

Bedon, C., Rinaldin, G., and Fragiacomo, M. (2015). "Non-linear modelling of the in-plane seismic behaviour of timber Blockhaus log-walls," *Engineering Structures* 91, 112-124. https://doi.org/10.1016/j.engstruct.2015.03.002

Cao, J., Li, X., and Liu, Y. (2023). "Seismic performance investigation of the Dou-gong joints of traditional Chinese timber structures," *European Journal of Wood and Wood Products* 81(1), 173-186. https://doi.org/10.1007/s00107-022-01863-x

Chen, C., Li, Y., Han, D., Kang, H., and Li, Y. (2025). "Simulation study on the static characteristics of 'Five-tier Outer Eave Column-head Dougong Bracket' from the main hall of Nanchan Temple in Tang Dynasty," *BioResources* 20(3), 6082-6099. https://doi.org/10.15376/biores.20.3.6082-6099

GB/T 15777 (2017). "Method for determination of the modulus of elasticity in compression parallel to grain of wood," Standardization Administration of China, Beijing, China.

GB/T 1933 (2009). "Method for determination of the density of wood," Standardization Administration of China, Beijing, China.

GB/T 1935 (2009). "Method of testing in compressive strength parallel to grain of wood," Standardization Administration of China, Beijing, China.

GB/T 1936.1 (2009). "Method of testing in bending strength of wood," Standardization Administration of China, Beijing, China.

GB/T 1939 (2009). "Method of testing in compression perpendicular to grain of wood," Standardization Administration of China, Beijing, China.

GB/T 1943 (2009). "Method for determination of the modulus of elasticity in compression perpendicular to grain of wood," Standardization Administration of

China, Beijing, China.
Lin, Y., Chun, Q., and Zhang, C. (2022). "Research on seismic performance of traditional Chinese hall-style timber buildings in the Song and Yuan dynasties (960–1368 AD): A case study of the main hall of Baoguo Temple," *Journal of Wood Science* 68(1), 608-621. https://doi.org/10.1186/s10086-021-02009-y
LY/T 3297 (2022). "Dynamic test method for shear modulus of wood," Standardization Administration of China, Beijing, China.
Meng, X., Li, T., and Yang, Q. (2019). "Experimental study on the seismic mechanism of a full-scale traditional Chinese timber structure," *Engineering Structures* 180, 484-493. https://doi.org/10.1016/j.engstruct.2018.11.055
Meng, X., Li, T., Yang, Q., and Wei, J. (2018). "Seismic mechanism analysis of a traditional Chinese timber structure based on quasi-static tests," *Structural Control and Health Monitoring* 25(10), article e2245. https://doi.org/10.1002/stc.2245
Niu, Q. (2017). *Experimental Study and Theoretical Analysis on Half-Scale Model of Timber Structure in Song Dynasty*, Master's Thesis, Taiyuan University of Technology, Taiyuan, China.
Sejkot, P., Aloisio, A., Obradović, V., and Iqbal, A. (2024). "Investigation into the hysteresis behavior of ductile connections utilizing nailed angle brackets for mass timber structures through experimental, finite element, and analytical methods," *Canadian Journal of Civil Engineering* 51(7), 803-811. https://doi.org/10.1139/cjce-2023-0394
Sha, B., Xie, L., Yong, X., and Li, A. (2021). "Hysteretic behavior of an ancient Chinese multi-layer timber substructure: A full-scale experimental test and analytical model," *Journal of Building Engineering* 43, 103-163. https://doi.org/10.1016/j.jobe.2021.103163
Song, X., Wu, Y., Li, K., Jin, L., Chen, F., Liu, X., and Dou, X. (2019). "Mechanical behavior of a Chinese traditional timber pagoda during construction," *Engineering Structures* 196, 109-302. https://doi.org/10.1016/j.engstruct.2019.109302
Suzuki, Y., and Maeno, M. (2006). "Structural mechanism of traditional wooden frames by dynamic and static tests," *Structural Control and Health Monitoring* 13(1), 508-522. https://doi.org/10.1002/stc.153
Van, D., and John, W. (2008). "Experimental investigation of the effect of multiple earthquakes on woodframe structural integrity," *Practice Periodical on Structural Design and Construction* 13(3), 111-117. https://doi.org/10.1061/(ASCE)1084-0680(2008)13:3(111)
Wang, J., Cui, Z., and Yu, L. (2022). "Analysis of the seismic behavior of traditional Chinese timber structures in the Tang Dynasty," *Structures* 41, 447-462. https://doi.org/10.1016/j.istruc.2022.05.007
Wu, C., Xue, J., Song, D., Ren, G., and Zhang, J. (2022). "Mechanical performance of inclined Dougong bracket sets under vertical load: experimental tests and finite element calculation," *Journal of Building Engineering* 45, 103-555. https://doi.org/10.1016/j.jobe.2021.103555
Wu, Y., Song, X., Ventura, C., and Lam, F. (2020). "Rocking effect on seismic response of a multi-story traditional timber pagoda model," *Engineering Structures* 209, 110-009. https://doi.org/10.1016/j.engstruct.2019.110009
Xue, J., Liang, X., Wu, C., Song, D., and Qi, L. (2022). "Experimental and numerical study on eccentric compression performance of Dou-Gong brackets at column tops," *Structures* 35, 608-621. https://doi.org/10.1016/j.istruc.2021.11.035

Yao, L., and Li, Y. (2023). "Simulation study on static characteristics of Qing-style 'One Bucket Three Liters' column-cap Dou-Gong bracket," *BioResources* 18(4), 6955-6970. https://doi.org/10.15376/biores.18.4.6955-6970

Yao, Z., Que, Y., Yang, X., Teng, Q., Li, Z., Zhang, X., Cai, W., Lu, H., Liu, Y., and Que, Z. (2019). "Status investigation and damage analysis of the Dougong under the external eaves of the main hall of Chuzu Tempel in the Shaolin Temple Complex," *BioResources* 14(2), 4110-4123. https://doi.org/10.15376/biores.14.2.4110-4123

Yeo, S., Hsu, M., Komatsu, K., Chung, Y., and Chang, W. (2016). "Shaking table test of the Taiwanese traditional Dieh-Dou timber frame," *International Journal of Architectural Heritage* 10(5), 539-557. https://doi.org/10.1080/15583058.2015.1009574

Zhang, B., Xie, Q., Li, S., Zhang, L., and Xue, J. (2023). "Numerical analysis of traditional Chinese timber structure: Simplified finite element model and composite elements of joints," *Journal of Building Engineering* 67, 106-027. https://doi.org/10.1016/j.jobe.2023.106027

Zhang, X., Cui, L., and Qi, H. (2024). "Seismic fragility analysis of traditional Chinese timber structures based on a simplified lumped mass model considering joint damage," *Structures* 70, 107-863. https://doi.org/10.1016/j.istruc.2024.107863

Article submitted: October 3, 2025; Peer review completed: February 13, 2026; Revised version received and accepted: March 4, 2026; Published: March 31, 2026.
DOI: 10.15376/biores.21.2.4357-4374